CrossMark

Synthetic zinc ferrite reduction by means of mixtures containing hydrogen and carbon monoxide

Eduardo Junca[1] · José Roberto de Oliveira[1] · Thomaz Augusto Guisard Restivo[2] · Denise Crocce Romano Espinosa[3] · Jorge Alberto Soares Tenório[3]

Abstract Solid waste generation is one of the main problems in the steelmaking process. One of the most problematic waste products is the electric arc furnace dust, which is a by-product rich in iron and zinc and is present as zincite (zinc oxide) or franklinite (zinc ferrite). This work focuses on the reduction kinetics of synthetic zinc ferrite by gases containing hydrogen and carbon monoxide. This process was examined via forced stepwise isothermal analysis. The test was conducted at temperatures ranging from 500 to 950 °C. Reduction of zinc was accomplished using a mixture of hydrogen and carbon monoxide in order to simulate reformed natural gas. The results indicated that reduction of zinc ferrite occurred in two stages (550–750 °C and 800–900 °C). The first stage was characterized by iron oxide reduction, where a mix control between nucleation and diffusion was determined. The apparent activation energy obtained was 71.5 kJ mol^{-1}. The second stage was characterized by zinc oxide reduction, where the controlling mechanism was identified as a mixed control between diffusion and phase boundary reaction. The apparent activation energy was 135.5 kJ mol^{-1}. The formation of a dense layer of metallic iron around the unreacted core may have caused the apparent activation energy to increase.

Introduction

The steel industry generates various types of solid waste, liquid and gaseous effluents such as slag, sludge, scrap and dust [1]. The electric arc furnace (EAF) is an important process broadly utilized to produce steel worldwide. During this process, dust is generated due to the explosion of CO and CO_2 bubbles or evaporation of high vapor pressure metals like zinc, lead and cadmium [2]. Researchers have been shown that the dust generated from electric arc furnace contain 4.8–23.5 % of zinc. These values can vary according to the raw material specific of the plant operation [3–5].

Zinc can be present in two forms, zinc oxide (ZnO) or zinc ferrite ($ZnFe_2O_4$). According to Menad [6], the zinc ferrite content depends on the zinc and iron content in the dust. Between 50 and 80 % of the zinc from the electric arc furnace dust is in the form of ZnO (zinc oxide), while the rest may be mixed with iron oxide, resulting in zinc ferrite ($ZnFe_2O_4$).

The study of zinc ferrite reduction is an important step to investigate the recovery of waste containing such phase, for example, electric arc furnace dust. Besides, reduction of zinc ferrite is characterized by generation of metallic iron, which can be reused in electric arc furnace to produce steel.

✉ Eduardo Junca
  eduardojunca@gmail.com

1   Federal Institute of Education Science and Technology of Espírito Santo, Av. Vitória, 1729 - Jucutuquara, Vitória, ES 29040-780, Brazil

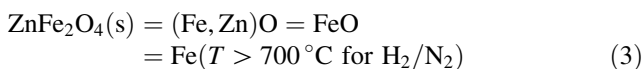2   University of Sorocaba, Rod. Raposo Tavares km 92.5, Sorocaba 18023-000, Brazil
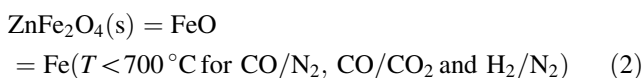
3   Department of Chemical Engineering, University of São Paulo, Av. Prof. Lineu Prestes, 580, São Paulo, SP 05424-970, Brazil

Solid–gas reactions are frequent in steelmaking. Iron oxide reduction by means of CO and H_2 are example of this kind of reaction. One way to obtain these gases is by steam natural gas reforming, via Eq. 1, in which produce 75 % of H_2 and 25 % of CO [6–8].

$$CH_4 + H_2O = 3H_2 + CO \qquad (1)$$

In this way, kinetic studies became important to know the mechanism during zinc ferrite reduction by H_2 and CO. Parameters like activation energy, pre-exponential coefficient and reaction order can be set up, which support the determination of operating parameters or dimensioning reactors, for example.

According to Tong and Hayes [9], the reduction of zinc ferrite by gaseous reactants containing CO and H_2 occurs via Eqs. 2 and 3.

$$ZnFe_2O_4(s) = FeO$$
$$= Fe(T < 700\,^{\circ}C \text{ for CO/N}_2, \text{CO/CO}_2 \text{ and } H_2/N_2) \qquad (2)$$

$$ZnFe_2O_4(s) = (Fe, Zn)O = FeO$$
$$= Fe(T > 700\,^{\circ}C \text{ for } H_2/N_2) \qquad (3)$$

In addition, the authors performed studies on zinc ferrite reduction using pure hydrogen and mixtures of nitrogen and hydrogen at temperatures between 700 to 900 °C. The authors stated that zinc ferrite reduction takes place in two stages. The first stage is the conversion of zinc ferrite into wustite, while the second stage is a slow reaction that involves the wustite reduction to iron.

Some authors [9] also performed zinc ferrite reduction studies using hydrogen as reducing gas. They explain that the reduction of zinc ferrite by hydrogen occurs in three stages. During the first stage, the zinc ferrite is reduced to magnetite (Fe_3O_4). The second stage is the reduction of the magnetite to wustite (FeO). In the third stage, the wustite is reduced to iron. The authors also calculated the activation energy involved in each stage, arriving to value of 118.02 kJ mol^{-1}, 174 kJ mol^{-1} and 92.48 kJ mol^{-1}, respectively.

Tong [10] performed reduction studies of pure zinc ferrite using mixtures of CO with CO_2 and argon. According to the author, $ZnFe_2O_4$ reduction with pure CO proceeds to an intermediate phase (wustite), rather than directly to the iron phase. The author goes on to state that the reduction of zinc ferrite to iron with CO–CO_2 and CO–N_2 mixtures, at temperatures above 570 °C, occurs in two stages. The first stage is the fast conversion of the zinc ferrite to wustite. The second stage entails a slow reaction involving the reduction of the wustite to porous or dense iron.

Some researchers [11] have cited that the zinc ferrite dissociates into zinc oxide and iron oxide. Then, both oxides are reduced simultaneously. Furthermore, the mechanisms involved in the reduction of zinc oxide and iron oxide by zinc ferrite dissociation can be compared with the mechanisms involved iron oxides reduction [9].

In addition, reduction of zinc oxides occurs via Eqs. 4 and 5 [12, 13].

$$ZnO(s) + H_2(g) = Zn(g) + H_2O(g) \qquad (4)$$

$$ZnO(s) + CO(g) = Zn(g) + CO_2(g) \qquad (5)$$
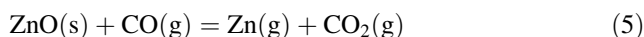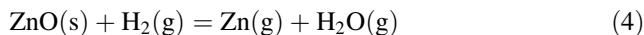
Other important studies also mention the reduction of zinc oxide, such as Gioia, Mura and Viola [14], Gonzáles et al. [15], Lew et al. [16], Guger and Manning [17], Zhang et al. [18], Kim et al. [19] and Zhang et al. [20].

The present paper aims to investigate the kinetics of synthetic zinc ferrite reduction by gaseous containing hydrogen and carbon monoxide applying a method called forced stepwise isothermal analysis.

Experimental

Zinc ferrite was synthesized by mixing analytical ZnO and Fe_2O_3 in the same proportion (1:1). This mixture was heating at room temperature up to 1000 °C for 5 h in ambient atmosphere. The ferrite phase formation was attested and characterized by X-ray analysis, scanning electron microscope (SEM) coupled with energy-dispersive X-ray detector (EDS), size analysis by laser diffraction and surface area per isotherms Brunauer, Emmett and Teller (BET) and Langmuir. Synthetic zinc ferrite pellets were prepared with 13 mm diameter, mass of 2 g and 53.1 % porosity.

Sample characterization

X-ray diffractions were to determine the main phases present in the synthetic ferrite. Besides, this technique was applied to determine phases present during the reduction tests. Analyses were performed in both synthetic zinc ferrite powder and pellets reduced up to 550, 700 and 850 °C. The assays were accomplished using a Rigaku diffractometer, Miniflex 300 model, equipped with Cu Kα ($\lambda = 15,418$ Å) tube. Step scan mode was applied to obtain the data. Additionally, scan range of 20°–100°, step width of 0.02° and duration time of 5 s were also used. To identify the phases on X-ray diffractions, JCPDF cards number 03-065-3111 for ZnO·Fe_2O_3, 01-079-0205 for ZnO, 01-075-0033 for Fe_3O_4, 01-089-0689 for FeO and 01-087-0722 for iron were used.

A Philips XL-30 scanning electron microscopy (SEM) was used to investigate the morphology of both synthetic zinc ferrite and reduced pellets. EDAX microprobe to X-ray spectrometric analysis was used in order to determine spot chemical analysis into synthetic zinc ferrite. The

pellet metallographic samples were grinded until center section. Synthetic zinc ferrite powder was mounted on double-faced. All samples were covered with gold.

Surface area was determined by BET (Brunauer–Emmett–Teller) through accelerated surface area and porosimetry system (ASAP 2020) equipment. A pre-treatment up to 200 °C for 24 h was necessary to accomplish the tests. Additionally, size analyses were performed via Mastersizer 2000. Such equipment uses laser diffraction technique to obtain the data.

Thermogravimetric and kinetic analysis

The experiments were carried out using a Setsys evolution Setaram thermobalance. Thermogravimetric technique applied was *Forced Stepwise Isothermal Analysis*, where the temperature and amount of time in each isotherm are pre-defined by operator [21].

Isotherms were set between 500 up to 950 °C with 50 °C intervals, several 15-min isotherms were programmed at each 50 °C. This cycle was adapted to the so-called *Forced Stepwise Isothermal Analysis* technique. The reducing gas contained hydrogen (75 %) and carbon monoxide (25 %), under 50, 100, 150 and 200 mL min^{-1}. Also, thermogravimetric analyses using different pellets sizes (8 and 13 mm) were performed to investigate the mass transfer effect into the pellets.

To perform the kinetic investigation, it was adopted the mechanisms shown in Table 1. These functions describe the main mechanisms of gas–solid reactions.

The control mechanism determination was aided through a comparison of the correlation factor (R^2) obtained from the $d(\alpha)/dt \times f(\alpha)$ plots drawn for each designed function. Then, the Arrhenius plots were sketched out for each previously determined mechanism to obtain the apparent activation energy.

Additionally, thermogravimetric analyses were quenched at 550, 700 and 850 °C to perform X-ray and scanning electron microscopy analyses. This step was necessary to investigate the phenomena during the reduction tests.

Results and discussion

Synthetic zinc ferrite characterization

X-ray analysis (Fig. 1) verified the synthesis indicating that 100 % of the sample was synthetic zinc ferrite.

Furthermore, scanning electron microscopy (Fig. 2) analysis indicates that the zinc ferrite has a porous aspect. Additionally, some EDS spectra were obtained from synthetic zinc ferrite. One of them can be seen in Fig. 3. It has just displayed the peaks for iron, zinc and oxygen. These results indicate that there are no impurities in the synthetic zinc ferrite.
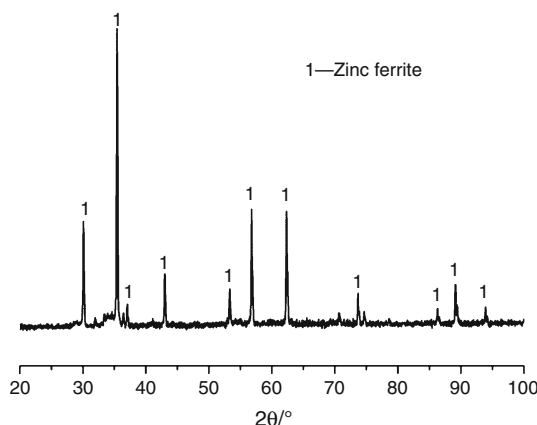

Fig. 1 X-ray diffraction pattern of synthetic zinc ferrite

Table 1 Mathematical suggestions for kinetic modeling for heterogeneous reactions of the gas–solid type [22, 23]

Mechanism	Symbol	Functions (α)
Phase boundary controlled	R2	$(1-\alpha)^{1/2}$
Phase boundary controlled	R3	$(1-\alpha)^{1/3}$
One-dimensional diffusion	D1	$\frac{1}{\alpha}$
Two-dimensional diffusion	D2	$\frac{1}{-\ln(1-\alpha)}$
Three-dimensional diffusion (Jander)	D3	$\frac{(1-\alpha)^{2/3}}{1-(1-\alpha)^{1/3}}$
Three-dimensional diffusion (Ginstling–Brounshtein)	D4	$\frac{1}{[(1-\alpha)^{-1/3}-1]}$
Two-dimensional nucleation	A2	$(1-\alpha)[-\ln(1-\alpha)]^{1/2}$
Three-dimensional nucleation	A3	$(1-\alpha)[-\ln(1-\alpha)]^{2/3}$
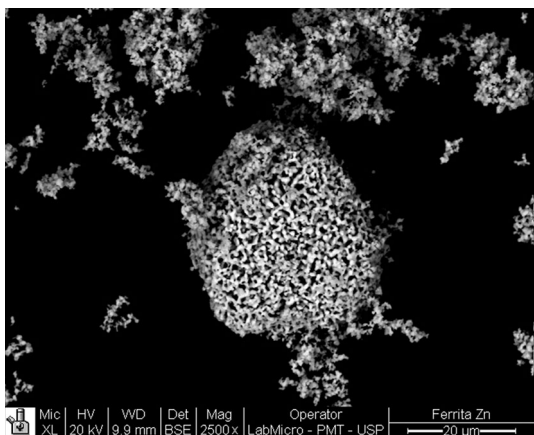
Fig. 2 Synthetic zinc ferrite image obtained by scanning electron microscopy

Additionally, spot chemical analysis (Table 2) also indicates that only Fe, Zn and O are present in synthetic zinc ferrite.
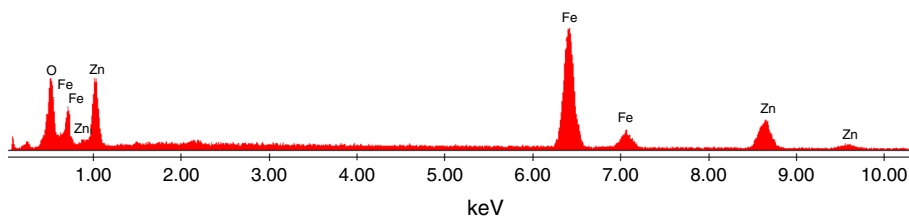
Size characterization indicates that the zinc ferrite particle ranges from 0.138 to 91.2 μm with 50 % of the particles smaller than 13.85 μm. Additionally, surface area of 1.27 m^2 g^{-1} was determined by BET analysis.

Effect of reducing gas flow and pellet size

Thermogravimetric analyses using different reducing gas flows were performed (Fig. 4) to investigate the transfer of the reducing gas to the pellet surface.

A minor increase in the reaction rate was observed with the increase of reducing gas flow (150–200 mL min^{-1}), indicating that the effect of gas transfer to the pellet surface does not interfere the reduction in this flow range. Additionally, Fig. 5 shows a faster complete conversion (total fraction reactes equals unity) with smaller pellet size during reduction tests. This result indicates that mass transfer into the pores is present on the reduction [24]. Furthermore, it was noted a change on reaction rate above 750 °C. Such result suggests a change in the control mechanism where the diffusion mechanism is more favored for higher temperature (>750 °C).

Table 2 Spot chemical analysis obtained of synthetic zinc ferrite via X-ray spectrometric

Components	Fe	Zn	O
Mass/%	48.9	29.7	21.4

—— Temperature/°C ···· 200/mL min^{-1} ··· 150/mL min^{-1} ‑ ‑ 100/mL min^{-1} ‑··‑ 50/mL min^{-1}
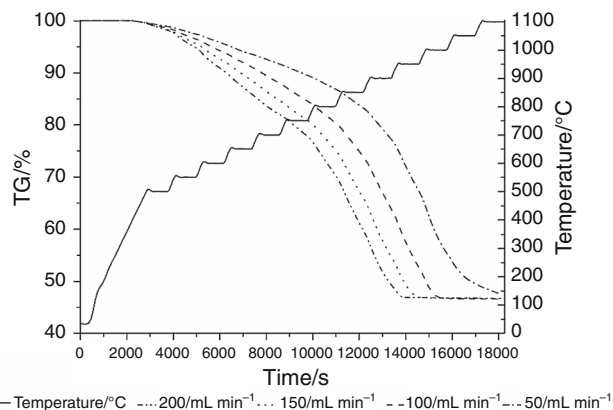
Fig. 4 Influence of the gas flow on the reaction rate
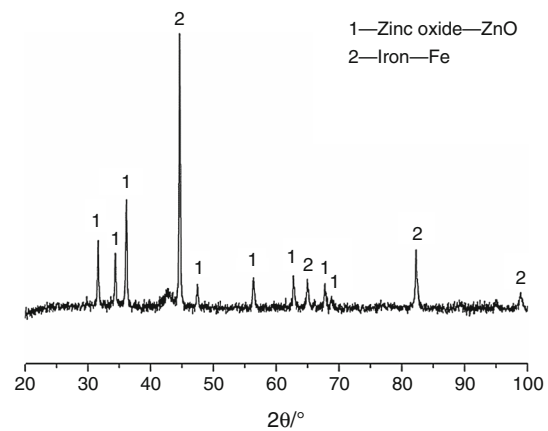

‑ ‑ ‑ 8 mm ······ 13 mm —— Temperature/°C
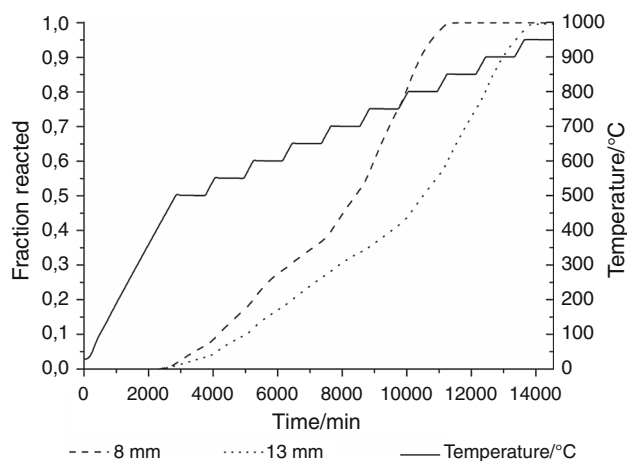
Fig. 5 Effect of pellets size on thermogravimetric analysis

Zinc ferrite reduction
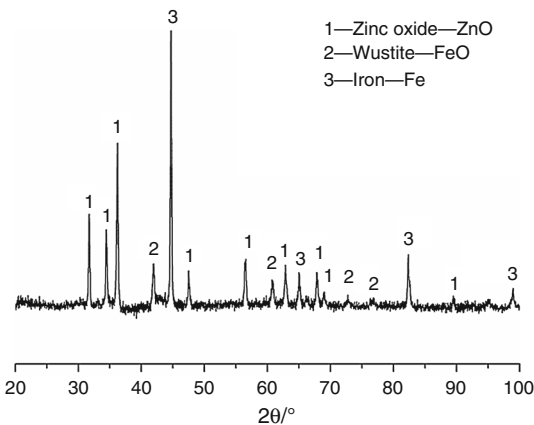
The zinc ferrite reduction is characterized by fast reduction to Fe$_3$O$_4$ and ZnO, as can be seen in Fig. 6, followed by iron oxide reduction to metallic iron.

Fig. 3 EDS spectrum of the synthetic zinc ferrite
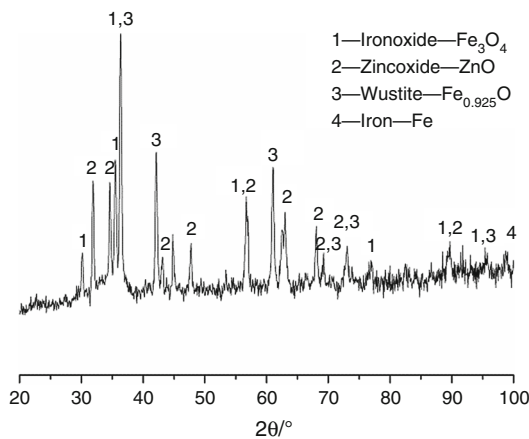
Fig. 6 X-ray diffraction patterns of zinc ferrite pellets reduced up to 550 °C

Fig. 8 X-ray diffraction patterns of zinc ferrite pellets reduced up to 850 °C

This process is characterized by a mass loss of approximately 20 %. The mass loss obtained in the first step of the process (up to 750 °C) was 22 % (Fig. 4), which is associated with $ZnFe_2O_4$ reduction to metallic iron and ZnO. This finding agrees with the results reported by Focht et al. [25]. Additionally, Fig. 7 shows X-ray diffraction patterns obtained for zinc ferrite pellet reduced up to 700 °C.

Peaks of ZnO, FeO and Fe were observed, which indicates that all Fe_3O_4 formed by zinc ferrite reduction is being reduced to FeO and Fe. The reduction of zinc oxide (ZnO) was observed for temperature above 750 °C. Figure 8 shows the X-ray diffraction patterns of zinc ferrite pellets reduced up to 850 °C.

X-ray diffraction analysis revealed that zinc oxide and iron were the main components of the pellets reduced up to 850 °C. This indicates that above 800 °C all iron oxide has already been reduced to Fe, while zinc oxide is still being

Fig. 7 X-ray diffraction patterns of zinc ferrite pellets reduced up to 700 °C

Table 3 Correlation factors from relation $d(\alpha)/dt \times f(\alpha)$ to functions cited in Table 1 at 550–750 °C

Temperature/°C	A2	A3	D1	D2	D3	D4	R2	R3
550	0.94	0.81	0.94	0.94	0.94	0.91	0.92	0.92
600	0.89	0.84	0.91	0.91	0.91	0.85	0.85	0.85
650	0.98	0.90	0.97	0.97	0.97	0.97	0.97	0.97
700	0.99	0.99	0.99	0.99	0.99	0.99	0.99	0.99
750	0.99	0.96	0.99	0.99	0.99	0.98	0.98	0.98

Table 4 Correlation factors from relation $d(\alpha)/dt \times f(\alpha)$ to functions cited in Table 1 at 800–900 °C

Temperature/°C	A2	A3	D1	D2	D3	D4	R2	R3
800	0.82	0.03	0.79	0.79	0.79	0.77	0.76	0.78
850	0.99	0.98	0.99	0.99	0.99	0.99	0.99	0.99
900	0.99	0.99	0.99	0.99	0.99	0.98	0.99	0.99
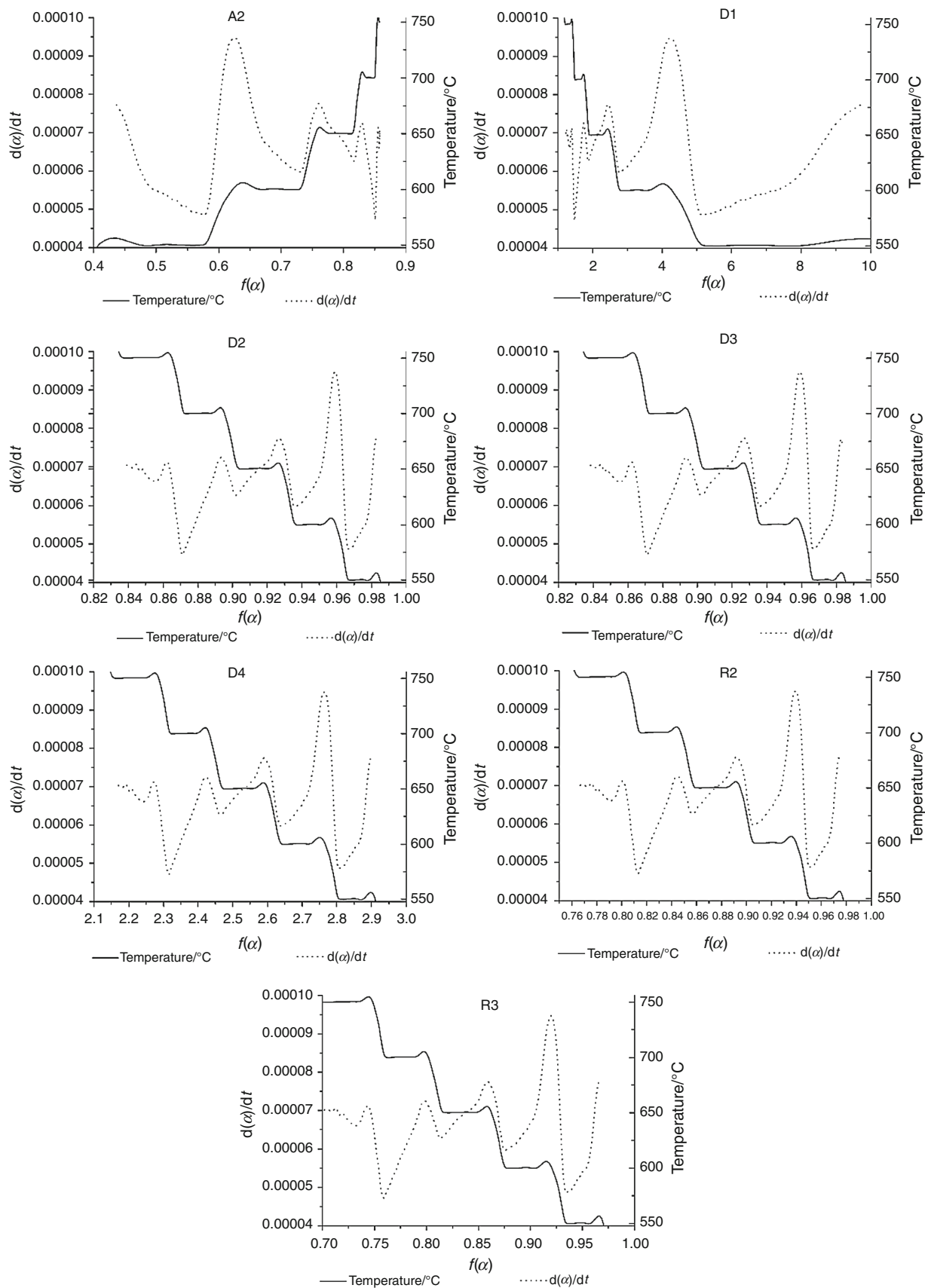
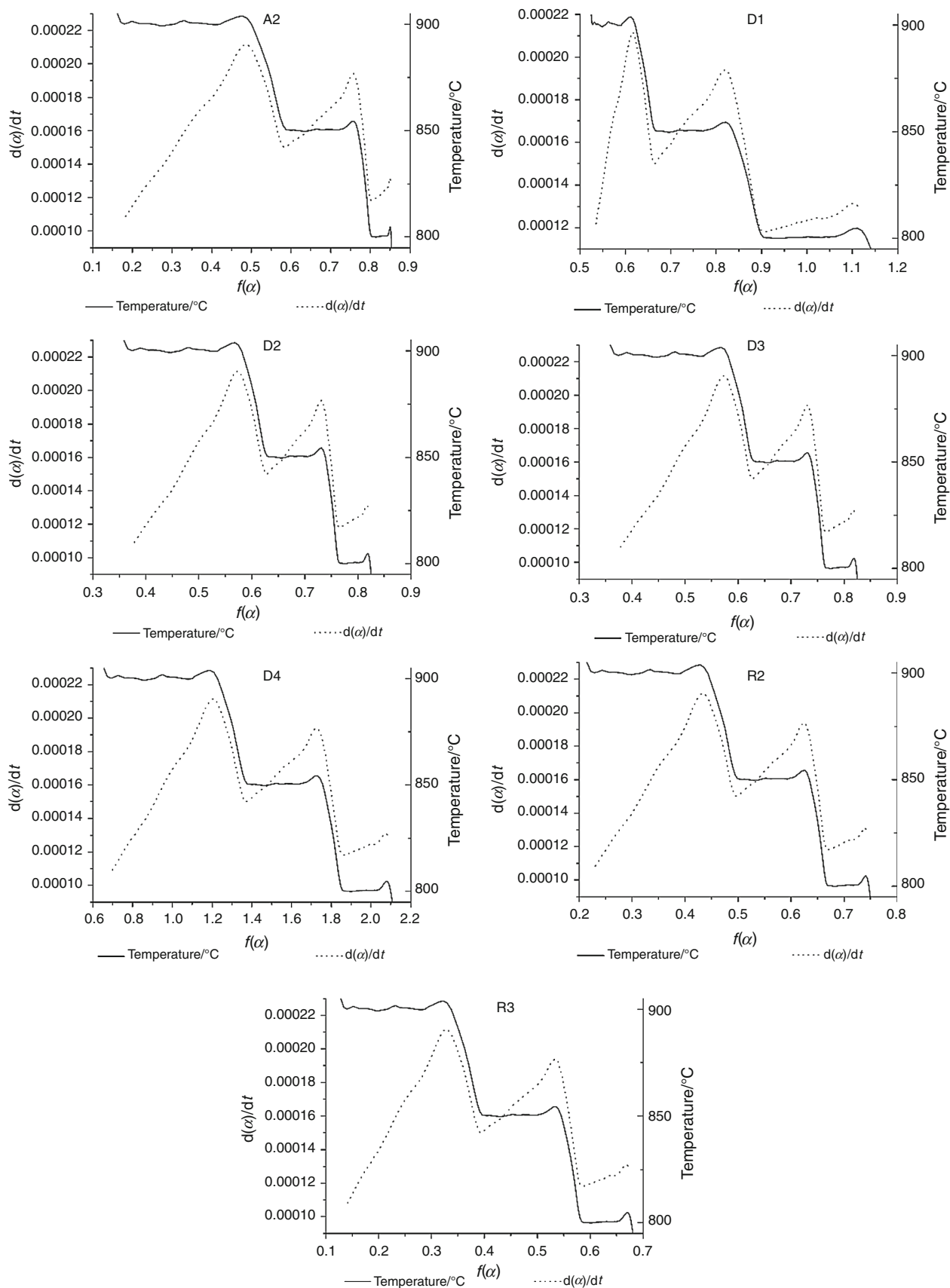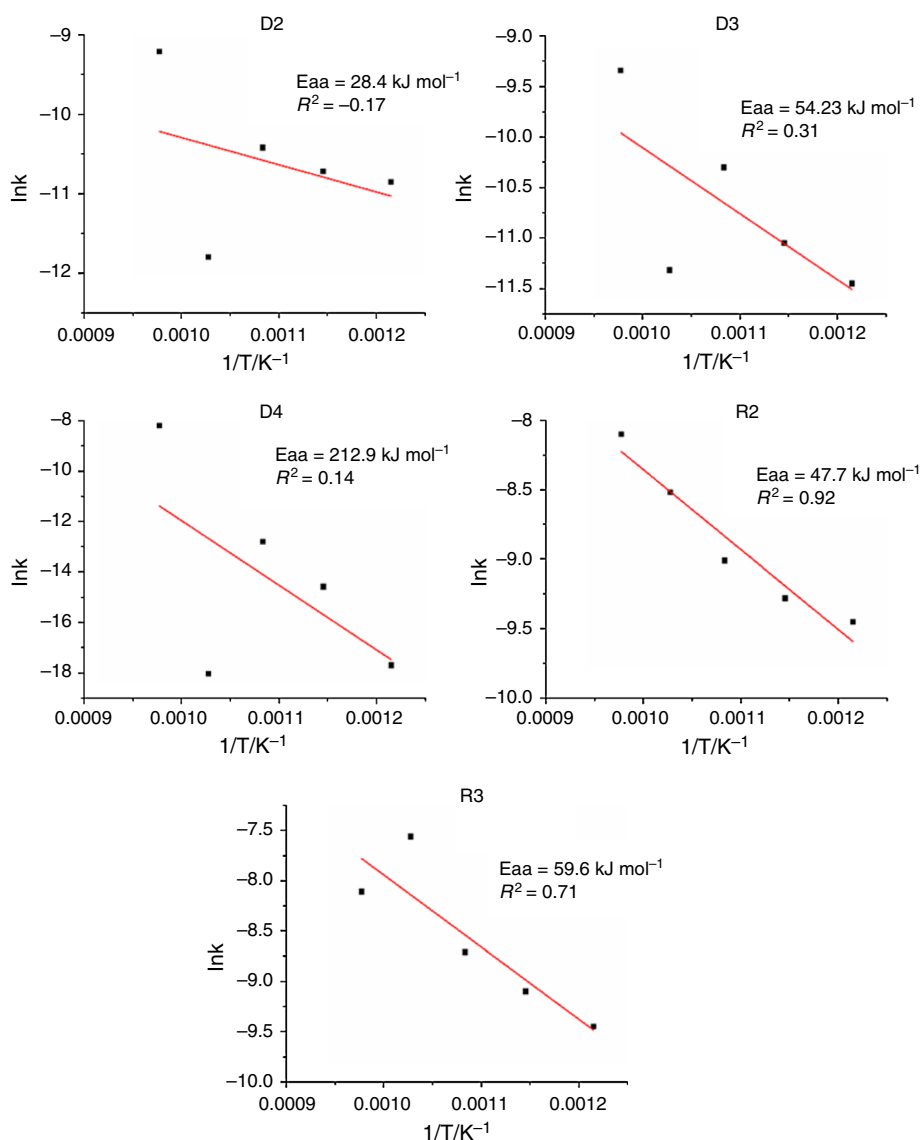**Fig. 9** Curves dα/dt × f(α) obtained for the functions A2, D1, D2, D3, D4, R2 and R3 at 550–750 °C

Fig. 10 Curves $d\alpha/dt \times f(\alpha)$ obtained for the functions A2, D1, D2, D3, D4, R2 and R3 at 800–900 °C

Fig. 11 Arrhenius plots obtained for the reduction of zinc ferrite pellets at 550–750 °C

reduced. Thermogravimetric analysis indicated a mass loss of 31.2 % (Fig. 4) in the second step, which by mass balance indicates the reduction of zinc oxide to gaseous zinc.

Kinetic investigation

Zinc ferrite reduction occurred in two steps (550–750 °C and 800–900 °C). Tables 3 and 4 show, respectively, the correlation factors for relationship $d(\alpha)/dt \times f(\alpha)$ and for all functions listed in Table 1 for both steps.

Table 3 e 4 indicates that the functions A2, D1, D2, D3, D4, R2 and R3 are probable controller mechanisms once greater correlation factors were obtained. Figures 9 and 10 show $d(\alpha)/dt$ as Y-axis and $f(\alpha)$ as X-axis plot with functions A2, D1, D2, D3, D4, R2 and R3 at 550–750 °C and 800–900 °C, respectively.

A critical analysis was performed on curves $d\alpha/dt \times f(\alpha)$ obtained from Fig. 9. It was determined that the functions D2, D3, D4, R2 and R3 showed greater correlation factors in the first step. In the same way, Fig. 10 shows the functions D2, D3 and R3 as the more linear ones for the second step, which makes these functions the probable controller mechanisms.

In order to search among controller mechanisms, Arrhenius plots were sketched out for the functions chosen via $d(\alpha)/dt \times f(\alpha)$ relationship. Figures 11 and 12 show the Arrhenius plots to functions D2, D3, D4, R2 and R3 (first step) and D2, D3 and R3 (second step), respectively.
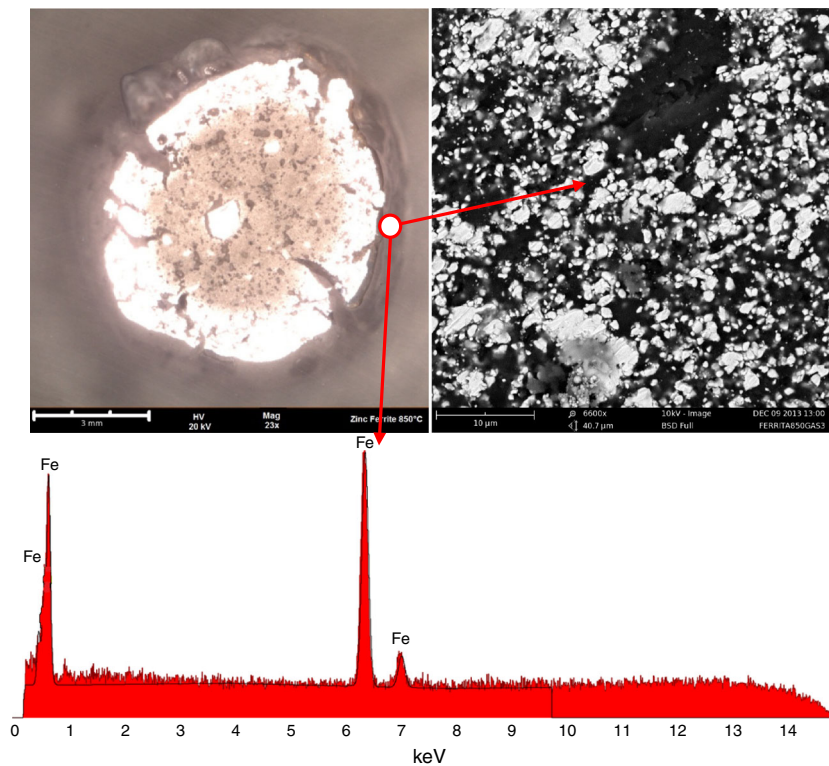
By Arrhenius plots, at 550–750 °C, the functions A2 (two-dimensional nucleation) and D1 (one-dimensional diffusion) showed greater correlation factors, which can indicates a mixed control. The apparent activation energy

Fig. 12 Arrhenius plots obtained for the reduction of zinc ferrite pellets at 800–900 °C
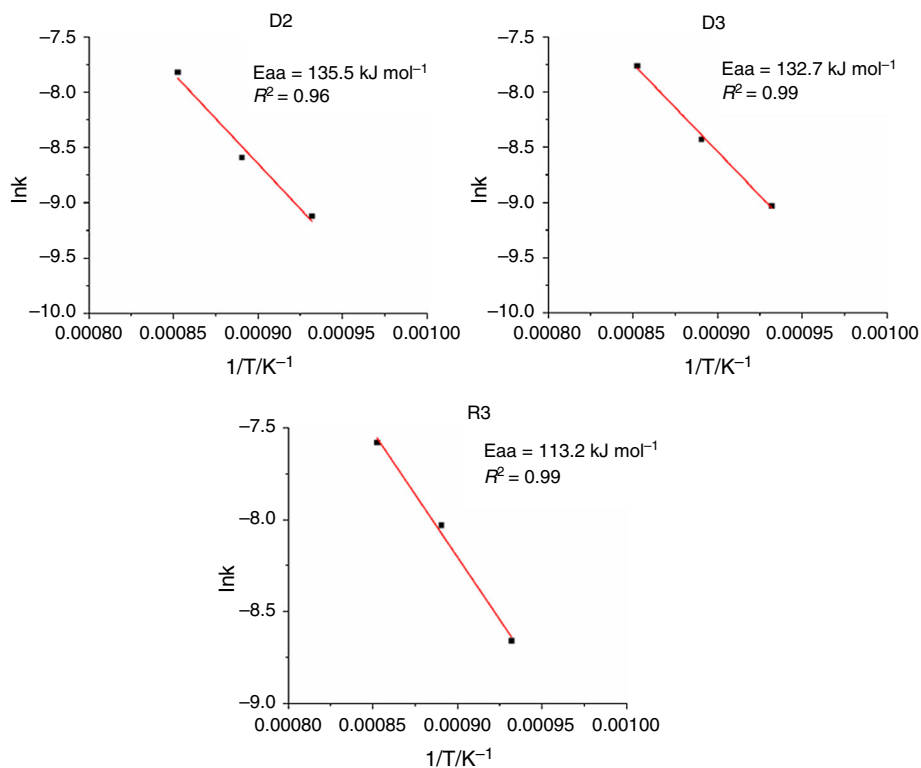
Fig. 13 SEM images and EDS spectrum obtained in the pellet of synthetic zinc ferrite reduced up to 850 °C

(Ea) determined in this step was 71.5 kJ mol^{-1}. Similar values of apparent activation energy were found in the literature. According to Lina, Chena and Li [26], the reduction of Fe$_3$O$_4$, an Ea of 70.4 kJ mol^{-1} was obtained. The controller mechanism was two-dimensional nucleation.

At 800–900 °C, it was noted that the functions D2, D3 and R3 showed greater correlation factors, which indicates a mixed control between two- and three-dimensional diffusion and phase boundary control. In this step, it was calculated an apparent activation energy of 135.5 kJ mol^{-1}. Besides, it was noted that above 750 °C, the diffusion phenomena is more present. The increase in the apparent activation energy may be due to the formation of dense layer of metallic iron around the unreacted core, as can be seen in Fig. 13.

Furthermore, the reduction of zinc ferrite pellets occurs from surface into the core. According to Yu et al. [27], this phenomenon is due to the reaction rate governed by gas diffusion through the sample. In addition, the iron layer formed around the unreacted core can hamper the diffusion for both the reducing gas into the pellet and the products formed outward pellet [28, 29].

Conclusions

Reducing gas transfer to the pellet surface has little influence for gas flow rates of 150 and 200 mL min^{-1}. The smaller the pellets diameter, the greater the reaction rate, which indicates the influence of the mass transfer into the porous in the reduction process for temperature upper 800 °C. Reduction of synthetic zinc ferrite occurred in two steps (550–750 °C and 800–900 °C). During the first step, it was observed the zinc ferrite reduction into iron oxide (Fe$_3$O$_4$) and zinc oxide (ZnO). Then, iron oxide is reduced to FeO and so to iron. In this step, it was determined a mixed control between two-dimensional nucleation and one-dimensional diffusion. The apparent activation energy obtained was 71.5 kJ mol^{-1}. The second step was associated with zinc oxide reduction where a layer of metallic iron is formed around the unreacted core of the pellet, blocking the gas diffusion into this layer. It was also determined a mixed control between two- and three-dimensional diffusion and phase boundary control. The apparent activation energy obtained was 135.5 kJ mol^{-1}.

References

1. Vieira CMF, Andrade PM, Maciel GS, Vernilli F Jr, Monteiro SN. Incorporation of fine steel sludge waste into red ceramic. Mater Sci Eng A. 2006;427:142–7.
2. Guézennec AG, Huber JC, Patisson F, Sessiecq P, Birat JP, Ablitze D. Dust formation by bubble-burst phenomenon at the surface of a liquid steel bath. ISIJ Int. 2004;44:1328–33.
3. Jarupisitthorn C, Pimtong T, Lothongkum G. Investigation of kinetics of zinc leaching from electric arc furnace dust by sodium hydroxide. Mater Chem Phys. 2002;77:531–5.
4. Martins FM, Neto JMR, Cunha CJ. Mineral phases of weathered and recent electric arc furnace dust. J Hazard Mater. 2008;154:417–25.
5. Soilic T, Mioc AR, Stefanovic SC, Radovic VN, Jenko M. Characterization of steel mill electric-arc furnace dust. J Hazard Mater B. 2004;109:59–70.
6. Olivier A, Vegliò F. Process simulation of natural gas steam reforming: fuel distribution optimisation in the furnace. Fuel Process Technol. 2008;89:622–32.
7. Izquierdo U, Barrio VL, Cambra JF, Requies J, Güemez MB, Arias PL, Kolb G, Zapf R, Gutiérrez AM, Arraibi JR. Hydrogen production from methane and natural gas steam reforming in conventional and microreactor reaction systems. Int J Hydrog Energy. 2012;37:7026–33.
8. Saito M, Kojima J, Iwai H, Yoshida H. The limiting process in steam methane reforming with gas diffusion into a porous catalytic wall in a flow reactor. Int J Hydrog Energy. 2015;40:8844–55.
9. Menad N, Ayala JN, Carcedo FG, Hernández A. Study of the presence of fluorine in the recycled fractions during carbothermal treatment of EAF dust. Waste Manag. 2003;23:483–91.
10. Tong LF, Hayes P. Mechanisms of the reduction of zinc Ferrites in H$_2$/N$_2$ gas mixtures. Miner Process Extract Metall Rev. 2007;28:127–57.
11. Liang M, Kang W, Xie K. Comparison of reduction behavior of Fe$_2$O$_3$, ZnO and ZnFe$_2$O$_4$ by TPR technique. J Nat Gas Chem. 2009;18:110–3.
12. Tong LF. Reduction mechanisms and behaviour of zinc ferrite-Part 1: pure ZnFe$_2$O$_4$. Miner Process Extr Metall. 2001;110:14–24.
13. Lee JJ, Lin CI, Chen HK. Carbothermal reduction of zinc ferrite. Mater Trans B. 2001;32B:1033–40.
14. Gioia F, Mura G, Viola A. Experimental study of the direct reduction of sinterized zinc oxide by hydrogen. Chem Eng Sci. 1977;32:1401–9.
15. González G, Jordens ZS, Escobedo S. Dependence of zinc oxide reduction rate on the CO concentration in CO/CO$_2$ mixtures. Thermochim Acta. 1996;278:129–34.
16. Lew S, Sarofim AF, Flytzani-Stephanopoulos M. The reduction of zinc titanate and zinc oxide solids. Chem Eng Sci. 1992;47:1421–31.
17. Guger CE, Manning FS. Kinetics of zinc oxide reduction with carbon monoxide. Metall Trans. 1971;2:3083–90.
18. Zhang YB, Su ZJ, Zhou YL, Li GH, Jiang T. Reduction kinetics of SnO$_2$ and ZnO in the tin, zinc-bearing iron ore pellet under a 20 %CO–80 %CO$_2$ atmosphere. Int J Miner Process. 2013;124:15–9.
19. Kim BS, Yoo JM, Park JT, Lee JC. A kinetic study of the carbothermic reduction of zinc oxide with various additives. Mater Trans. 2006;47:2421–6.
20. Zhang B, Yan XY, Shibata K, Uda T, Tada M, Hirasawa M. Thermogravimetric-mass spectrometric analysis of the reaction between oxides (ZnO, Fe$_2$O$_3$ or ZnFe$_2$O$_4$) and polyvinyl chloride under inert atmosphere. Mater Trans JIM. 2000;41:1342–50.

21. Junca E, Restivo TAG, Espinosa DCR, Tenório JAS. Application of stepwise isothermal analysis method in the kinetic study of reduction of basic oxygen furnace dust. J Therm Anal Calorim. 2015;120:1913–9.

22. Chen F, Sorensen OT, Meng G, Peng D. Thermal decomposition of $BaC_2O_4 \cdot 0.5\ H_2O$ studied by stepwise isothermal analysis and non-isothermal thermogravimetry. J Therm Anal. 1998;53:397–410.

23. Maqueda LAP, Ortega A, Criado JM. The use of master plots for discriminating the kinetic model of solid state reactions from a single constant-rate thermal analysis (CRTA) experiment. Thermochim Acta. 1996;277:165–73.

24. Yu D, Zhu M, Utigard TA, Barati M. TG/DTA study on the carbon monoxide and graphite thermal reduction of a high-grade iron nickel oxide residue with the presence of siliceous gangue. Themochim Acta. 2014;575:1–11.

25. Focht GD, Ranade PV, Harrison DP. High-temperature desulfurization using zinc ferrite: reduction and sulfidation kinetics. Chem Eng Sci. 1988;43:3005–13.

26. Lina HY, Chena YW, Li C. The mechanism of reduction of iron oxide by hydrogen. Thermochim Acta. 2003;400:61–7.

27. Yu D, Zhu M, Utigard TA, Barati M. TGA kinetic study on the hydrogen reduction of an iron nickel oxide. Miner Eng. 2013;54:32–8.

28. Moukassi M, Steinmetz P, Dupre B, Gleitzer C. Mechanism of reduction with hydrogen of pure wustite single crystals. Metall Trans B Process Metall. 1983;14B:125–32.

29. Wiltowski T, Piotrowski K, Lorethova H, Stonawski L, Mondal K, Lalvani SB. Neural network approximation of iron oxide reduction process. Chem Eng Process Process Intensif. 2005;44:775–83.